TURBULENT DECAY BEHIND MULTI-SCALE AND CONVENTIONAL GRIDS

Per-Åge Krogstad
Dept. Energy and Process Engineering, Norwegian University Science and Technology
Trondheim, Norway

Peter Davidson
Dept. Engineering, Cambridge University
Cambridge, U.K.

ABSTRACT

We investigate wind tunnel turbulence generated by a conventional and two multi-scale grids. The conventional and multi-scale grids were all designed to produce turbulence with the same integral scale, so that a direct comparison could be made between the different flows. The turbulent decay rate behind our multi-scale grids is virtually identical to that behind the equivalent conventional grid. In particular, all flows exhibit a power-law decay of energy, $u^2 \sim t^{-n}$, where n is very close to the classical Saffman exponent of $n = 6/5$. Our results are at odds with some other experiments performed on multi-scale grids, where significantly higher energy decay exponents and turbulence levels have been reported.

1 Introduction

In recent years a number of wind-tunnel experiments and numerical simulations have focused on quasi-homogeneous turbulence generated by multi-scale grids. (See, for example, Hurst & Vassilicos [3], and Nagata *et al.* [7].) Classical theories for grid turbulence predict that the energy decays as $\langle \mathbf{u}^2 \rangle \sim t^{-n}$ and predicts that homogeneous turbulence can decay no faster than $n \sim 10/7$. In some of these experiments the turbulence appears to behave in unexpected ways. For example, Hurst & Vassilicos [3] report unusually high values decay exponents ($n \sim 2$ rather than the classical $n \sim 1.2 \rightarrow 1.4$), and also exponential decay rate has been observed for some grid geometries.

However, this suggestion is somewhat at odds with the evidence of direct numerical simulations in periodic cubes, where it is usually found that, after some transient, the behavior of the turbulence is largely independent of the precise form of the initial energy spectrum (see, for example, Ossai & Lesieur [8]). Indeed, it is often argued that, once fully developed, all the turbulence remembers of its initial conditions is the prefactor, c_m, in the expression $E(k \rightarrow 0) = c_m k^m$, c_m being an invariant for $m \leq 4$ (Ossai & Lesieur, [8], Davidson, [1], Ishida *et al.*, [4], and Davidson, [2]).

In order to test the hypothesis that turbulence behind multiscale grids will develop in a non-classical way, a series of wind tunnel experiments using two multi-scale grids were investigated and the results compared with data obtained using a similar conventional grid. In order to ensure that the comparison is meaningful, the dimensions of the grids were chosen such that the integral scale of the turbulence some short distance downstream of each grid, ℓ_0, is virtually the same in all three cases (to within a percent or so). The experiments were carried out in a large working section, and measurements taken over the extended range $80\ell_0 < x < 400\ell_0$, which translates to $50M < x < 240M$ for the conventional grid. The turbulence generated by all three grids is virtually identical. In particular, there is no significant difference in the behavior of Re_λ, and in all cases the decay exponent n is very close to the classical prediction of Saffman [9], i.e. $n = 6/5$.

2 The Experimental Set-up

The experiments were performed in the large recirculating wind tunnel described in Krogstad & Davidson [6]. The tunnel test-section has transverse dimensions of 2.7m x 1.8m (measured at the start of the test section) and is 12m long. There is an adjustable roof to compensate for the growth of the sidewall boundary layers and the grids were mounted upstream in the test section contraction to improve isotropy. From the location of the grid to the entrance of the test section, the area contraction ratio was 1.48 and the test section starts $x = 1.2m$ downstream of the grid.

All three grids were produced from 2mm thick sheet metal. The conventional grid (labeled *cg*) has square holes 30mm x 30mm punched at 40mm spacing, giving a mesh size of $M = 40mm$, a bar width of $t = 10mm$, and a solidity of $\sigma = 44\%$. The tests on this grid were all performed at a Reynolds number of $Re_M = UM/\nu = 3.6 \times 10^4$, where U = 13.5m/s was the mean speed in the tunnel.

The first of the multi-scale grids (labeled *msg*1) is similar to the cross-grid-type(a) of [3] and is shown in Figure 1(a). It has bar widths ranging from $t_1 = 8mm$ down to $t_3 = 2mm$, and mesh sizes ranging from $M_1 = 64mm$ to $M_3 = 15mm$. The solidity of *msg*1 is also $\sigma = 44\%$. These measurements were taken at U = 14.0m/s. The second multi-scale grid (*msg*2) is

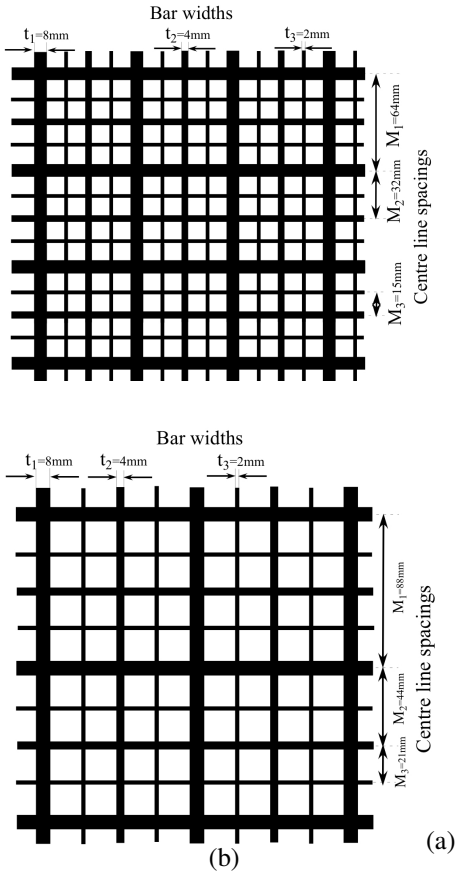

Figure 1. The two multi-scale grids used in this study.

shown in Figure 1(b). As for $msg1$, the bar widths vary from $t_1 = 8mm$ down to $t_3 = 2mm$, though the mesh sizes are larger, with $M_1 = 88mm$ to $M_3 = 21mm$. This reduces the solidity of $msg2$ to $\sigma = 33\%$. This grid was tested at U = 15.5m/s.

The turbulence produced by these grids becomes more-or-less homogeneous and fully developed at around $x = 2m$, at which point the Kolmogorov microscale is $\eta \approx 0.22mm \rightarrow 0.26mm$. On the other hand, the integral scales at $x = 2m$, $\ell_0 = \ell(x = 2m)$, turn out to be $\ell_0 = 23.9mm$ (for cg), $\ell_0 = 23.6mm$ (for $msg1$), and $\ell_0 = 23.4mm$ (for $msg2$), respectively. Note that the geometric length-scales associated with the two multi-scale grids almost span the range of dynamic scales associated with the turbulence, from around 9η up to several integral scales. Finally we note that, in terms of ℓ_0, the tunnel cross-section is approximately $115\ell_0 \times 80\ell_0$, thus ensuring that there is minimal influence of the side-wall boundary layers.

The data was obtained using single and two component hot-wire anemometry. For the measurements of the decay of $\left\langle (u_x)^2 \right\rangle$, spectra, the length scales η and ℓ etc. a purpose made $2.5\mu m$ partly etched Platinum-10%Rhodium straight single wire probe was produced. The active wire length was $0.5mm$. For two component measurements and for global checks such as spanwise homogeneity etc. an X-wire probe with $\pm 45^o$ nominal wire angles was produced. For this probe $5\mu m$ partly etched wires were used with $1mm$ wire lengths. The two wires were also separated in the spanwise direction by $\Delta z = 1mm$. By careful handling of the two delicate probes

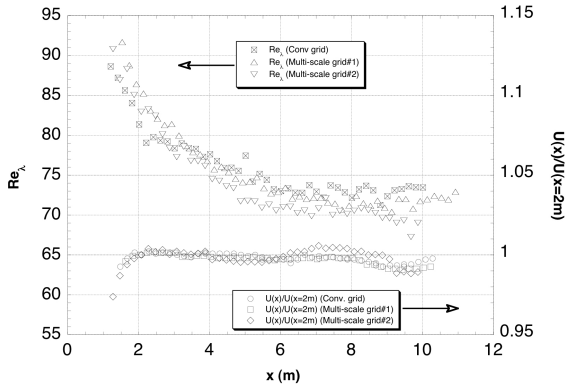

Figure 2. Streamwise distributions of Re_λ (left axis) and the test section centre-line speed, U, (right axis). U is normalized by U at $x = 2m$.

it was possible to maintain the same wires throughout the whole experiment. Hence there should be no effects in the data that can be attributed to changes in probe characteristics.

The probes were operated at an overheat temperature of about 320 degrees using in-house manufactured anemometers which were tuned to a frequency response f_w of at least 20kHz. The output from the anemometers were suitably offset and amplified to span as much as possible of the ± 10 volt range of the 16 bit acquisition card used before the signals were passed through an AC coupled Krohn-Hite amplifier and low-pass filter unit. The filter frequency f_c was set by inspecting the dissipation spectra of a few initial measurements with very high filter settings. f_c was then set at the frequency where noise first started to affect the dissipation spectra and a new set of data was obtained at a sampling frequency which was slightly higher than $2f_c$.

For verification purpose only, a number of two component laser Doppler anemometry (LDA) measurements were taken for each grid, but these data were not used in the data analysis presented here. Further information about the instrumentation and data analysis may be found in [6].

3 Tests for Homogeneity and Isotropy.

Since the grids were mounted inside the contraction, the first development was under the influence of a favourable pressure gradient, but for $x > 2m$, U was constant to within $\pm 0.5\%$ (see Figure 2), with $Re = U\ell_0/\nu = 2.1 \times 10^4$, 2.2×10^4 and 2.4×10^4, respectively, for the three grids. Figure 2 also shows the streamwise variation of $Re_\lambda = \left\langle u_x^2 \right\rangle^{1/2} \lambda/\nu$ for all three grids. The present values are only about one third of those reported by Hurst & Vassilicos [3] and there is no significant difference between the conventional and multi-scale grids.

The spanwise distributions of the turbulence intensity, $T_u = u/U$, where $u = \left\langle u_x^2 \right\rangle^{1/2}$, measured at $x \approx 2m$ and $x \approx 6m$ are shown in Figure 3. The measurements were made over a span corresponding to about $z \approx \pm 4M$, where M represents the largest mesh of each grid. Since M is only a well defined scaling length for the conventional grid, we have chosen to scale z with ℓ_0, hence the apparent differences in the measurement ranges in the figure. All three grids are seen to behave in

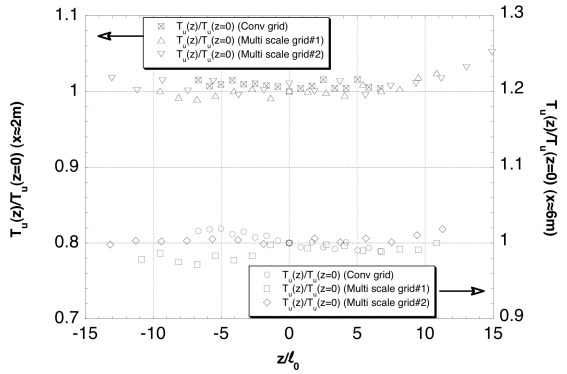

Figure 3. Spanwise distributions of T_u at $x \approx 2m$ (left axis) and $x \approx 6m$ (right axis).

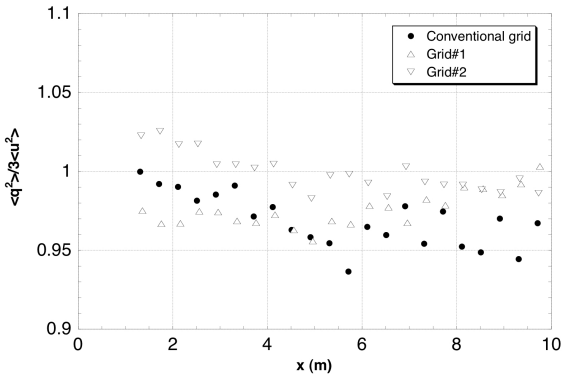

Figure 4. Streamwise distributions of $\langle q^2 \rangle / 3 \langle u_x^2 \rangle$.

a similar manner, with variations in T_u limited to about $\pm 3\%$ at $x = 2m$ and $\pm 2\%$ at $x = 6m$. We conclude that, for $x > 2m$, the turbulence is relatively homogeneous.

The streamwise development of the anisotropy of the turbulence, as measured by the ratios $\langle u_x^2 \rangle / \langle u_y^2 \rangle$, $\langle u_x^2 \rangle / \langle u_z^2 \rangle$ and $\langle q^2 \rangle / 3 \langle u_x^2 \rangle$, where $\langle q^2 \rangle = \langle \mathbf{u}^2 \rangle = \langle u_x^2 + u_y^2 + u_z^2 \rangle$, was measured for each grid (Figure 4). For all cases it was found to follow closely the distributions reported for the conventional grid in Figure 3 of [6]. We show here just the three streamwise developments of $\langle q^2 \rangle / 3 \langle u_x^2 \rangle$ which is seen to be very similar for the 3 cases and the ratio is very close to the isotropic value of 1. For all grids $\langle u_x^2 \rangle / \langle u_y^2 \rangle$, $\langle u_x^2 \rangle / \langle u_z^2 \rangle$ and $\langle q^2 \rangle / 3 \langle u_x^2 \rangle$ were close to unity at $x = 2m$, but $\langle u_x^2 \rangle / \langle u_y^2 \rangle$ and $\langle u_x^2 \rangle / \langle u_z^2 \rangle$ were found to divert slowly with increasing x. The largest departure from isotropy was observed at the exit of the test section, where $\langle u_x^2 \rangle / \langle u_z^2 \rangle$ reached values in the range of 0.8 to 0.9. There was a corresponding growth in $\langle u_x^2 \rangle / \langle u_y^2 \rangle$, to produce the almost constant $\langle q^2 \rangle / 3 \langle u_x^2 \rangle$ ratios shown in the figure.

Figure 5 shows the skewness and flatness distributions of the streamwise fluctuations measured along the centre line of the test section. The flatness is constant throughout the measurement range at $F_u \approx 2.95$ for all grids. The skewness is slightly different for the grids initially, as was shown in Figure **??**, but they all tend steadily towards $S_u \to 0$ as the flow develops downstream.

In most of what follows we shall restrict the analysis of

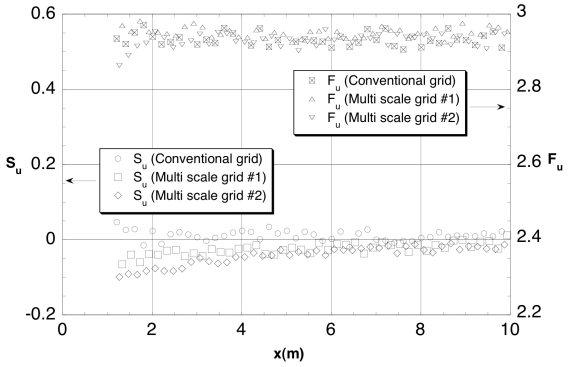

Figure 5. Streamwise distributions of skewness and flatness factors.

our data to the region $x > 2m$, to avoid any acceleration effects caused by the inhomogeneities in U, and to $x < 8m$, because of the increased levels of noise for large x as the turbulence level drops well below 1%. For completeness, however, the full set of data will be included in the plots so that the reader may see where and how the data departs from classical decay behavior. From the data presented above we see that, in this range, the turbulence is reasonably homogeneous and that, although there is some anisotropy, the levels are not excessive and are comparable to, if not better, than in most other experiments.

4 The Energy Decay Rate.

As noted in Davidson ([1] and [2]) and Krogstad &Davidson [6], there are two classical predictions for n. One arises when $E(k \to 0) \sim k^2$, a situation called Saffman turbulence, and the other when $E(k \to 0) \sim k^4$, so-called Batchelor turbulence. Self similarity of the large scales (when it applies) demands

$$u^2 \ell^3 = \text{constant} \,, \quad (\text{for Saffman turbulence}) \,, \tag{1}$$

$$u^2 \ell^5 = \text{constant} \,, \quad (\text{for Batchelor turbulence}) \,. \tag{2}$$

These may be combined with the empirical, but well supported, law

$$\frac{du^2}{dt} = -A \frac{u^3}{\ell} \,, \; A = \text{constant} \,, \tag{3}$$

to give $n = 6/5$ (Saffman's exponent; see Saffman [9]) in $E(k) \sim k^2$ turbulence, and $n = 10/7$ (Kolmogorov's exponent; see Kolmogorov [5]) in $E(k) \sim k^4$ turbulence. The first of these exponents was observed in the experiments of Krogstad &Davidson [6] and the second in the numerical simulations of [4]. While other decay exponents have been proposed from time to time, it is natural to keep these two classical predictions in mind when examining the experimental data. However, there is a slight complication which arises when comparing these predictions with experiments: in wind tunnel data the coefficient A can vary slowly along the test section, and

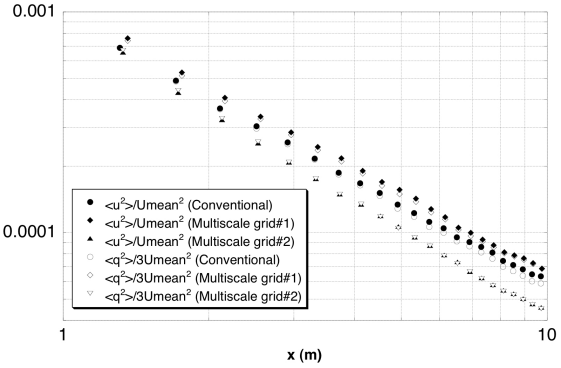

Figure 6. Streamwise distributions of $\langle u_x^2 \rangle / U^2$ (filled symbols) and $\langle q^2 \rangle / 3U^2$ (open symbols).

this causes slight departures from the ideal values of $n = 6/5$ or $n = 10/7$, even when Eq. (1) or (2) hold true (see Krogstad &Davidson [6]). Indeed, we shall see shortly that just such a slow variation of A occurs in our experiments.

Let us now estimate the decay exponents for our three grids by comparing the experimental data with the power law

$$\frac{\langle u_x^2 \rangle}{U^2} = a \left[\frac{x - x_0}{\ell_0} \right]^{-n} \Rightarrow \ln \left[\frac{\langle u_x^2 \rangle}{U^2} \right] = \ln a - n \ln \left[\frac{x - x_0}{\ell_0} \right] \tag{4}$$

where, as before, ℓ_0 is the integral scale at $x = 2m$. It is notoriously difficult to obtain reliable estimates of n. First, we do not know in advance where x_0 will lie. Second, if the range of x/ℓ_0 is too short, the decay exponent becomes very sensitive to the choice of the unknown x_0. Third, if data from the inhomogeneous region close to the grid is included in the fit, then higher (and misleading) values of n are usually obtained. Fourth, for large x/ℓ_0 the turbulence intensity is low, so that noise starts to become problematic, obvious sources being unsteadiness in the fan speed caused by the feed-back regulation system, electronic noise in the instrumentation and pressure fluctuations arising from the side-wall boundary layers. In summary, then, to obtain reliable estimates of n we require that: (i) x_0 be chosen systematically and with care; (ii) there is an extended x/ℓ_0 range; (iii) anomalous data close to the grid must be excluded; and (iv) data for large x/ℓ_0 should be ignored when the noise level becomes excessive.

Figure 6 shows $\langle u_x^2 \rangle / U^2$ and $\langle q^2 \rangle / 3U^2$, obtained using two different alignments of the x-wires, all plotted as a function of x. This log-log plot demonstrates that, for all three grids, there is a clear power-law relationship between u^2 and x. It also shows that $\langle u_x^2 \rangle$ and $\langle q^2 \rangle$ follow essentially the same power law. In view of the difficulty in obtaining reliable estimates of n, three different fitting procedures were used and their results compared. All three methods are described in detail in [6] and the data obtained from the fits are shown in Table 4. The essence of method M1 is to do a regression analysis of the data using the logarithmic form in Eq. 4 by sorting out the range of the data points which produces the lowest variance in the fit. This is a conventional Regression method. In method M2 we use the fact that a large number of data was obtained with very small streamwise increments. This allowed the exponent to be obtained using a 3 point discretization scheme directly on the data. This was called the Local exponent method. Finally a method called the Maximum decay range method was used. In this procedure a range of x_0 was tested in Eq. 4 and compared to the measurements. The value of x_0 which produced the widest range of constant decay exponent n was deemed to be the correct one and the corresponding exponent is shown in Table 4. Full details of the fit methods are given in Krogstad & Davidson [6].

	x_0	n	n	n
	M1	M1	M2	M3
Conv. grid	0.26m	1.13	1.14	1.17
Grid 1	0.43m	1.12	1.17	1.19
Grid 2	0.30m	1.25	1.25	1.23

Table 1. Estimates of the energy decay exponent n obtained using three different methods, M1, M2 and M3 (see description in text).

There are three striking features of Table 1. First, all three grids yield decay exponents very close to the classical Saffman value of $n = 6/5 = 1.2$. Second, the conventional and multi-scale grids produce almost identical results (to within experimental uncertainty). Third, these decay exponents are a long way from the n in the range 1.7 to 2.0 quoted in [3] for their four fractal cross grids. It is likely, therefore, that all three of our grids produce Saffman turbulence.

We demonstrated that the exponents derived agree closely with Saffman turbulence. However, there is some scatter in the various estimates for the decay exponents which implies that we cannot exclude other forms of decay. If we pre-empt our discussion of length scales in § 5, we may check if the data also satisfy the requirements of Eqs. 1 or 2. Figure 7 shows the streamwise development of $\langle u_x^2 \rangle \ell^3 / U^2 \ell_0^3$ and $\langle u_x^2 \rangle \ell^5 / U^2 \ell_0^5$ for all three grids. The data is plotted for the range $2 < (x - x_0) < 10$m. Recall that, in Saffman turbulence, self-similarity of the large scales requires $u^2\ell^3$ = constant, as distinct from, say, Batchelor turbulence, in which $u^2\ell^5$ = constant. It is clear from Figure 7 that $u^2\ell^3$ is indeed more or less constant in all three cases while $u^2\ell^5$ increases steadily downstream. The trend is undisputable for the conventional grid, but the trend for multiscale grid 1 is not as clear as for the other grids. The scatter in this data is largely a consequence of the difficulty associated with estimating ℓ, as will be discussed in § 5.

Finally we consider the dimensionless dissipation coefficient A in Eq. (3), which is normally taken to be constant during the decay of isotropic turbulence. Assuming isotropy at the small scales, the viscous dissipation rate, ε, can be written as

$$\varepsilon = \frac{3}{2} \frac{A u^3}{\ell} = 15\nu \left\langle \left(\frac{\partial u_x}{\partial x} \right)^2 \right\rangle , \tag{5}$$

which allows us to estimate A from measurements of $\left\langle (\partial u_x / \partial x)^2 \right\rangle$, u and ℓ. The corresponding values of A are plotted in Figure 8 for all three grids as a function of

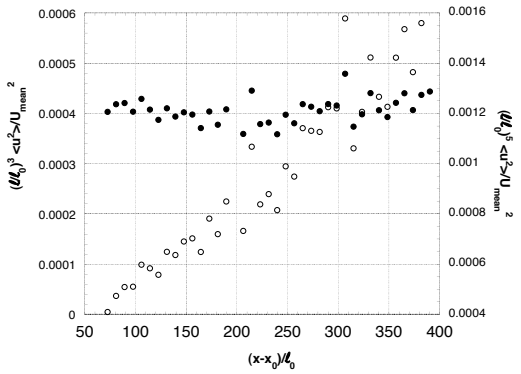

a)

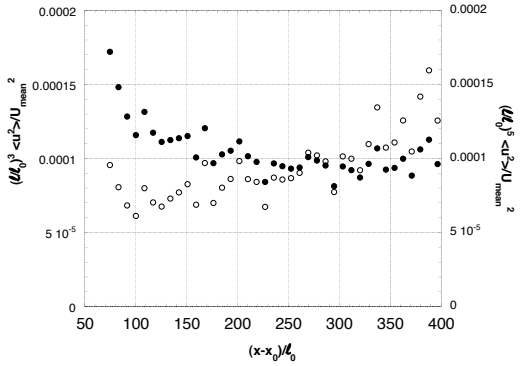

b)

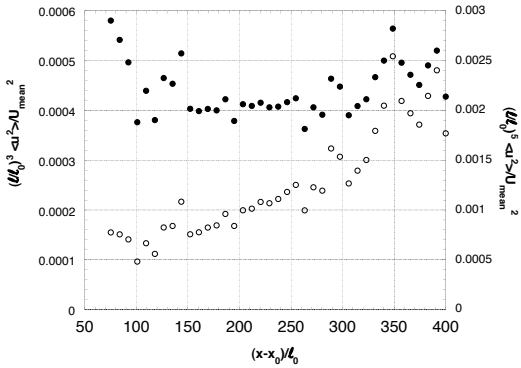

c)

Figure 7. $\langle u_x^2 \rangle \ell^3/U^2\ell_0^3$ and $\langle u_x^2 \rangle \ell^5/U^2\ell_0^5$ versus $(x-x_0)/\ell_0$ for all three grids. a) Conventional grid, b) msg1, c) msg2.

$(x-x_0)/\ell_0$. Again, there is some scatter, largely due to the difficulty in estimating ℓ. Never-the-less, once the turbulence is fully developed, say for $(x-x_0)/\ell_0 > 100$, there is a slow but steady decline in A which is consistent across all three grids. As noted earlier, this slow variation in A means that, even if we have Saffman turbulence, with $u^2\ell^3$ = constant, we need not recover $n = 6/5$, as this value of n relies on A being strictly constant.

5 The Development of Length Scales

We now turn to the length scales η, λ and ℓ. The Kolmogorov microscale, defined as $\eta = \left(\nu^3/\varepsilon\right)^{1/4}$, can be determined from the isotropic estimate of dissipation in Eq. (5) or

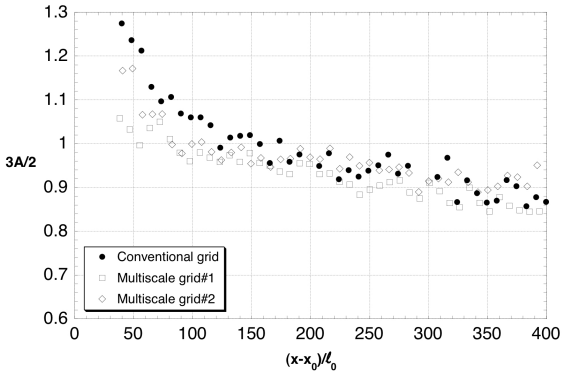

Figure 8. Streamwise development of A obtained from Eq. (5).

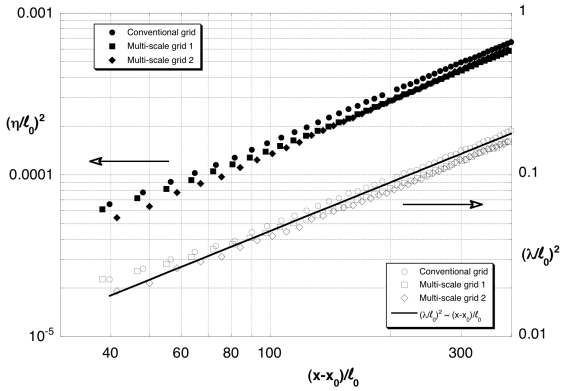

Figure 9. Streamwise distributions of η^2 (filled symbols) and λ^2 (open symbols). The straight line is $\lambda^2 \sim (x-x_0)$.

from the decay rate of $\langle q^2 \rangle$, both estimates giving virtually identical estimates for η in this type of flow, as demonstrated by [6]. The streamwise development of the Kolmogorov and Taylor microscales, η^2 and λ^2, are shown in Figure 9.

Noting that combining Eq. (3) and (4) yields

$$\lambda^2 = \frac{10\nu\ell}{Au} = \frac{10\nu(x-x_0)}{nU}\,, \tag{6}$$

we see that λ^2 should scale as $\lambda^2 \sim (x-x_0)$, which is indeed verified in Figure 9. This is, in effect, confirmation of a power-law form of energy decay.

The integral scale, ℓ, is defined in the usual way as $\ell = \int_0^\infty \frac{\langle u_x(x)u_x(x+r)\rangle}{\langle u_x^2\rangle} dr = \int_0^\infty f(r)dr$, where $f(r)$ is the usual longitudinal correlation function and, in practice, $\langle u_x(x)u_x(x+r)\rangle$ is evaluated using Taylor's hypothesis. Ideally $f(r)$ should decay monotonically to zero for large r, but in experiments $f(r)$ almost always exhibits a weak oscillatory tail which persists for many multiples of ℓ. This makes it difficult to evaluate $\int_0^\infty f(r)dr$ accurately since it will depend on where the integral is terminated, and so the integral was only taken up to the first zero crossing, which introduces a small systematic error. As a result, there is some uncertainty in the calculated values of ℓ. Our estimates of ℓ for all three grids are shown in Figure 10.

Evidently, ℓ exhibits considerably more scatter than η

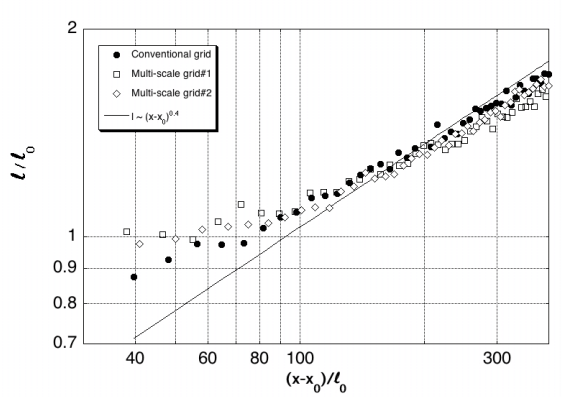

Figure 10. The integral scale, ℓ, as a function of $(x-x_0)/\ell_0$. The solid line is $\ell \sim (x-x_0)^{0.4}$.

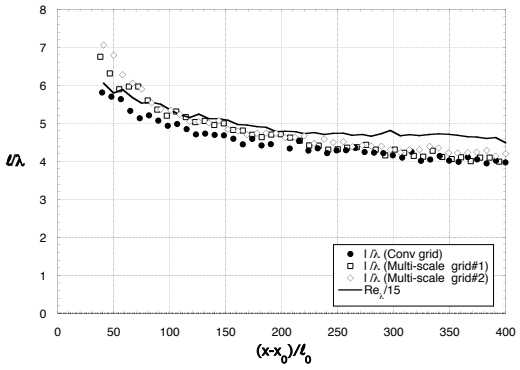

Figure 11. Ratio of length scales, ℓ/λ.

or λ, but it is clear that the development of ℓ is similar for all three grids and follows a power law. Moreover, power-law energy decay with constant A demands $\ell \sim ut$, and so Saffman turbulence predicts $\ell \sim (x-x_0)^{0.4}$, provided we ignore the slow decline in A. This is shown in Figure 10 for comparison and the data for all cases follow such a trend for $(x-x_0)/\ell >$ 100.

Finally we demonstrate that the data presented is internally consistent. It follows from Eqs. 3 and 5 that the ratio $\ell/\lambda = ARe_\lambda/10$ for homogeneous and locally isotropic turbulence. In Figure 11 the ℓ/λ data has been plotted. Also included is the line $ARe_\lambda/10$ assuming that A is constant with $3A/2 \approx 1$. Accounting for some streamwise variation in A as demonstrated in Figure 8 which will shift the line slightly up for $(x-x_0)/\ell_0 < 100$ and down by about 10% for $(x-x_0)/\ell_0 > 100$, the agreement is seen to be very good, confirming that the flow must be close to the homogeneous approximation implied in the data analysis.

6 Conclusions

Our primary findings are two-fold. First, it seems that Saffman's decay law is reasonably robust, since the energy decay exponents for all three grids are close to Saffman's classical prediction of n = 6/5. Second, the multi-scale grids used here produce almost identical results to the equivalent classical grid. In particular, all three flows exhibit remarkably similar streamwise distributions of Re_λ (Figure 2), flatness and skewness (figure 5), and dimensionless decay coefficient A (Figure 8). It is also worth noting that the spectra for the multiscale grids exhibit classical Kolmogorov scaling, with $E(k)$ collapsing on ℓ and u at low k, and on η and υ at high k.

Our findings contradict those of some previous studies which report unusual behavior behind similar multi-scale grids, in particular, a very high energy decay exponent of around $n \sim 2.0$ and unusually high values of Re_λ. A decay exponent of $n \sim 2.0$ is particularly worrying as the theoretical maximum for n (assuming the dimensionless decay coefficient, A, is constant) is n = 10/7. However, these earlier measurements were taken much closer to the grid where the flow exhibits initial grid-dependent inhomogeneities; inhomogeneities which, according to the present data, disappear further downstream.

REFERENCES

[1] DAVIDSON, P.A. 2004 *Turbulence, An introduction for Scientists and Engineers*, Oxford University Press.

[2] DAVIDSON, P.A. 2009 The role of angular momentum conservation in homogenous turbulence. *J. Fluid Mech.* **632**, 329–358.

[3] HURST, D. & VASSILICOS, J.C. 2007 Scalings and decay of fractal-generated turbulence. *Phys. Fluids* **19**, (3), 035103.

[4] ISHIDA, T., DAVIDSON, P.A. & KANEDA Y. 2006 On the decay of isotropic turbulence. *J. Fluid Mech.* **564**, 455–475.

[5] KOLMOGOROV, A.N. 1941 On the degeneration of isotropic turbulence in an incompressible viscous fluid. *Dokl. Akad. Nauk. SSSR* **31**, (6), 538–541.

[6] KROGSTAD, P.-Å. & DAVIDSON, P.A. 2010 Is grid turbulence Saffman turbulence? *J. Fluid Mech.* **642**, 373–394.

[7] NAGATA, K., SUZUKI, H., SAKAI, Y., HAYASE, T. & KUBO, T. 2008 Direct numerical simulation of turbulence characteristics generated by fractal grids. *Int. Review Phys.* **2**, (6), 400–409.

[8] OSSAI, S. & LESIEUR, M.M. 2000 Energy backscatter in large-scale simulations of three dimensional incompressible isotropic turbulence. *J. Turbulence* **1**, 010.

[9] SAFFMAN, P.J. 1967 The large-scale structure of homogeneous turbulence. *J. Fluid Mech.* **27**, 581–593.